Inorganic Chemistry

pubs.acs.org/IC

Forum Article

Physicochemical Factors That Influence the Deoxygenation of Oxyanions in Atomically Precise, Oxygen-Deficient Vanadium Oxide Assemblies

Brittney E. Petel and Ellen M. Matson*

Cite This: *Inorg. Chem.* 2021, 60, 6855−6864

Read Online

ACCESS | Metrics & More | Article Recommendations | Supporting Information

ABSTRACT: Here, we report our findings related to the structural and electronic considerations that influence the rate of oxygen-atom transfer (OAT) to oxygen-deficient polyoxovanadate alkoxide (POV-alkoxide) clusters ($[V_6O_6(OC_2H_5)_{12}]^n$; n = 1−, 0, 1+). A comparison of the reaction times required for the reduction of nitrogen-containing oxyanions (NO_x^-, x = 2, 3) by the POV-ethoxide cluster in its anionic (**1-$V_6O_6^{1-}$**; $V^{III}V^{IV}_5$), neutral (**4-$V_6O_6^0$**; $V^{III}V^{IV}_4V^V$), or cationic (**6-$V_6O_6^{1+}$**; $V^{III}V^{IV}_3V^V_2$) charge state reveals that OAT is significantly influenced by three factors: (1) ion-pairing interactions between the POV-alkoxide and the negatively charged oxyanion; (2) oxidation states of remote vanadyl ions in the Lindqvist assembly; (3) the steric bulk surrounding the coordinatively unsaturated V^{III} ion. This work provides atomic-level insight related to structure−function relationships that govern the rate of OAT at metal oxide surfaces using polyoxometalate clusters as molecular models.

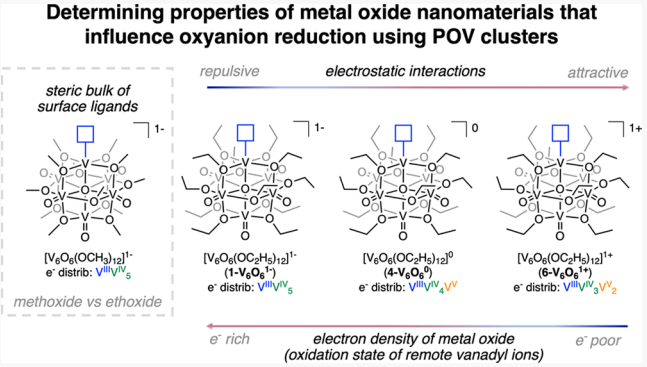

INTRODUCTION

Oxygen-atom transfer (OAT) is an important step in the deoxygenation of chemical contaminants and organic substrates.[1−3] Heterogeneous catalysts, such as reducible metal oxides, have displayed high activity for these types of industrially relevant transformations, often invoking the formation of surface oxygen-atom vacancies, and consequently, unsaturated reduced metal ions, during catalysis.[3−5] Theoretical and spectroscopic reports have elucidated that, in many redox-active transition metal oxides, the oxidation state of the vacancy-bearing metal ion does not depend on the oxidation states of the metal ions in the pristine oxide. For example, analysis of the electronic consequences of oxygen-atom removal in both V_2O_5 (V^V)[6,7] and VO_2 (V^{IV})[8−10] presents evidence for metal reduction to vanadium(III) at the defect site. Given the consistent oxidation state of the vacancy-bearing metal center (e.g., V^{III}), discrepancies in the reactivity of these materials are attributed to differences in the oxidation states of the *remote* transition metal ions that compose the bulk solid (e.g., V^V vs V^{IV}; Figure 1). However, probing the consequences of modifying the oxidation states of single metal ions surrounding defect sites within reducible metal oxides would require a targeted electronic control that is not possible in bulk materials.

Additional considerations in optimizing the OAT reactivity of metal oxides focus on the structure and charge of surface ligands (Figure 1).[11−14] Indeed, the applicability of these systems toward various industries (e.g., medicine, photocatalysis, batteries, etc.) are dependent on properties such as size, shape, crystallinity, and dispersion, all of which can be modified by introducing organic functionalities at the surface of a metal oxide nanomaterial. Additionally, ligands have been cited to control the surface charge of nanoparticles, influencing the way these materials interact with ions in solution.[14−16] To date, little is known regarding how these properties, collectively, influence the OAT reactivity at metal oxide surfaces.

Given the current limitations in controlling the physicochemical properties of extended solids with atomic precision, researchers have turned to the use of homogeneous multinuclear clusters as model complexes.[17−27] The goal of these studies rests on gaining a fundamental understanding of the factors that influence the reactive sites in catalytic systems. In particular, polyoxometalates (POMs) have emerged as promising homogeneous models for extended solids. Like bulk metal oxides, these three-dimensional polynuclear assemblies are composed of redox-active transition metal

Special Issue: Heterogeneous Interfaces through the Lens of Inorganic Chemistry

Received: July 11, 2020
Published: September 14, 2020

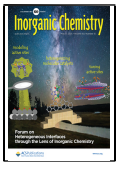

https://dx.doi.org/10.1021/acs.inorgchem.0c02052
Inorg. Chem. 2021, 60, 6855−6864

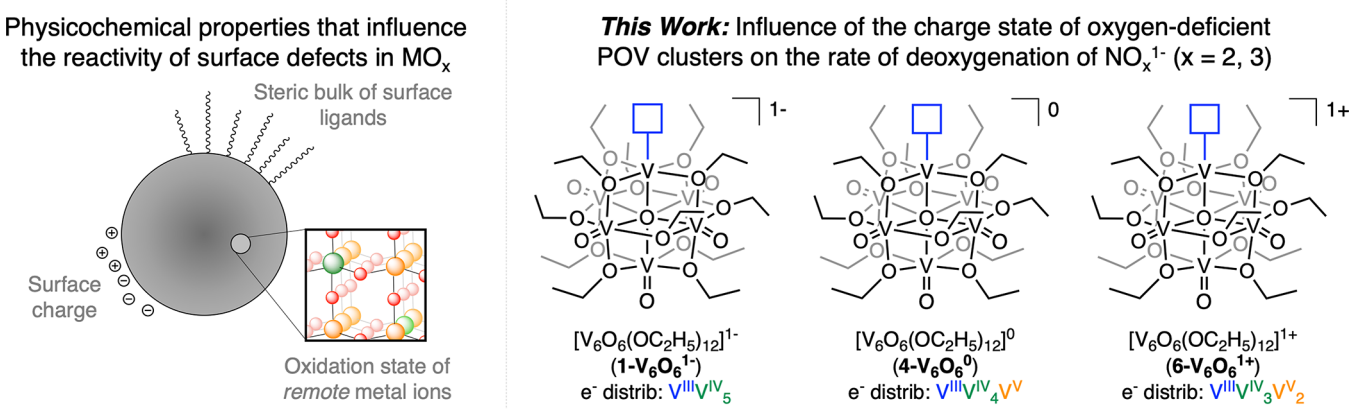

Figure 1. Physiochemical properties that influence the reactivity of metal oxides, including surface ligands, surface charge, and the oxidation state of remote metal ions surrounding the catalytically active metal center (left). Key: red, oxygen; green, vanadium; orange, remote vanadyl ions. Here, we present a structure−function study using a redox series of oxygen-deficient POV-alkoxide clusters to analyze the influence of the charge state, steric bulk, and electrostatic interactions on OAT from nitrogen-containing oxyanions (right).

ions (e.g., vanadium, molybdenum, tungsten, tantalum, niobium, etc.), linked together by bridging oxygen atoms.[28,29] Generally, these systems exhibit rich electronic structures that present the ability to mediate multielectron redox processes.[17−25,27,29−36] With relevance to gaining molecular-level insight into the reactivity of heterogeneous metal oxide systems, the mechanism of OAT reactivity with POMs has been indirectly investigated and is speculated to undergo a mechanism similar to that of OAT chemistry with extended solids (e.g., the Mars−van Krevelen mechanism).[4]

Toward the development of atomically precise models for extended solids, our research group has focused on a special class of metal oxide clusters, namely, Lindqvist polyoxovanadate alkoxide (POV-alkoxide) clusters.[31−35] Characterization of the molecular composition and electronic structure has revealed that these polynuclear assemblies are ideal candidates for modeling bulk vanadium oxide.[37−39] With a vanadium oxide core featuring six terminal V═O moieties, bridged by alkoxide ligands, the structure of the Lindqvist metal oxide closely resembles the surface structure of V_xO_y. Furthermore, the bridging alkoxide ligands impart enhanced solubility to the hexavanadate core in organic solvents, rendering these assemblies suitable as homogeneous models for MO_x surface chemistry.

The electrochemical profile of these alkoxypolyoxovanadium clusters features four, quasi-reversible, one-electron redox events that encompass five charge states of the Lindqvist assembly (Figure S1 and Scheme S1).[37−39] For example, the addition of 1 equiv of an oxidant to the most reduced form of the cluster, $[V_6O_7(OR)_{12}]^{2-}$ (e^- distrib. V^{IV}_6), results in isolation of the Lindqvist cluster in a charge state that is one-electron-oxidized in comparison to that of the starting material (i.e., $[V_6O_7(OR)_{12}]^{1-}$; e^- distrib. $V^{IV}_5V^{V}$). Characterization by infrared (IR) and electronic absorption spectroscopies, as well as X-ray crystallography and bond-valence-sum calculations, unambiguously confirmed formation of this monoanionic cluster. The subsequent addition of oxidants results in sequential one-electron oxidation of the metal oxide cluster, presenting access to a redox series of mixed-valent POV-alkoxides, $[V^{IV}_xV^{V}_{6-x}O_7(OR)_{12}]^n$. The ability for the Lindqvist cluster to undergo multiple redox reactions reveals that the hexavanadate core functions as a "redox reservoir" able to store electrons across the six delocalized vanadium centers. Indeed, all five clusters have been isolated and characterized, allowing for the systematic investigation of the influence of the cluster electronics on reactivity.

Given this unique structural and electronic tunability, we have explored the use of POV-alkoxide clusters as systems for modeling vacancy formation at the surface of reducible metal oxides. In particular, we have discovered methods for isolating rare examples of oxygen-deficient metal oxide clusters, $[V_6O_6(OR)_{12}]^n$ (n = CH_3, C_2H_5), synthesized via V═O bond cleavage and cluster reduction.[31−35] These vacancy-containing vanadium oxide assemblies possess coordinatively unsaturated vanadium(III) ions that mimic the electronic structure of oxygen defect sites in vanadium(IV) and -(V) oxides.

Additionally, these oxygen-deficient assemblies have been shown to be reactive in OAT chemistry for the activation of small molecules[30,31] and organic substrates.[32] Recently, we have disclosed that the addition of NO_x^- (x = 2, 3) to the anionic, monovacant POV-methoxide cluster, $[V_6O_6(OCH_3)_{12}]^{1-}$, results in the quantitative formation of nitric oxide via OAT from the substrate to the oxygen-deficient Lindqvist assembly to yield the fully oxygenated species, $[V_6O_7(OCH_3)_{12}]^n$ (n = 1−, 2−).[30] Interested in expanding our understanding of the role of the cluster charge state on OAT in small-molecule activation processes, we targeted the investigation of NO_x^- reduction by a redox series of oxygen-deficient POV-alkoxide clusters, $[V_6O_6(OCH_3)_{12}]^n$ (n = 1−, 0, 1+). However, given the instability of the POV-methoxide cluster in its neutral charge state, $[V_6O_6(OCH_3)_{12}]^0$,[33] we turned our attention to a series of monovacant POV-*ethoxide* clusters. Fortuitously, our group has demonstrated the isolation of oxygen-deficient vanadate assemblies featuring bridging ethoxide ligands across a range of oxidation states, $[V_6O_6(OC_2H_5)_{12}]^n$ (n = 1−, 0, 1+).[32,34,35] This renders these clusters distinctly qualified to probe the influence of changes in the oxidation state of remote transition metal ions, which ultimately results in a change of the cluster reduction potential (Figure 1, right). Spectroscopic investigations have revealed that the site-differentiated vanadium(III) center retains its oxidation state across all three charge states of the cluster.

Here, we report the OAT reactivity of a series of monovacant POV-ethoxide clusters, $[V_6O_6(OC_2H_5)_{12}]^n$ (n = 1−, 0, 1+) toward the deoxygenation of nitrite (NO_2^-) and

https://dx.doi.org/10.1021/acs.inorgchem.0c02052
Inorg. Chem. 2021, 60, 6855−6864

Scheme 1. Addition of NO_2^- to 1-$V_6O_6^{1-}$ Resulting in a Mixture of Cluster-Containing Products, 2-$V_6O_7^{2-}$ and 3-$V_6O_6NO^{1-}$ (Right), and Trapping the Byproduct, NO, with CoTPP Resulting in the Sole Formation of 2-$V_6O_7^{2-}$ (Left)

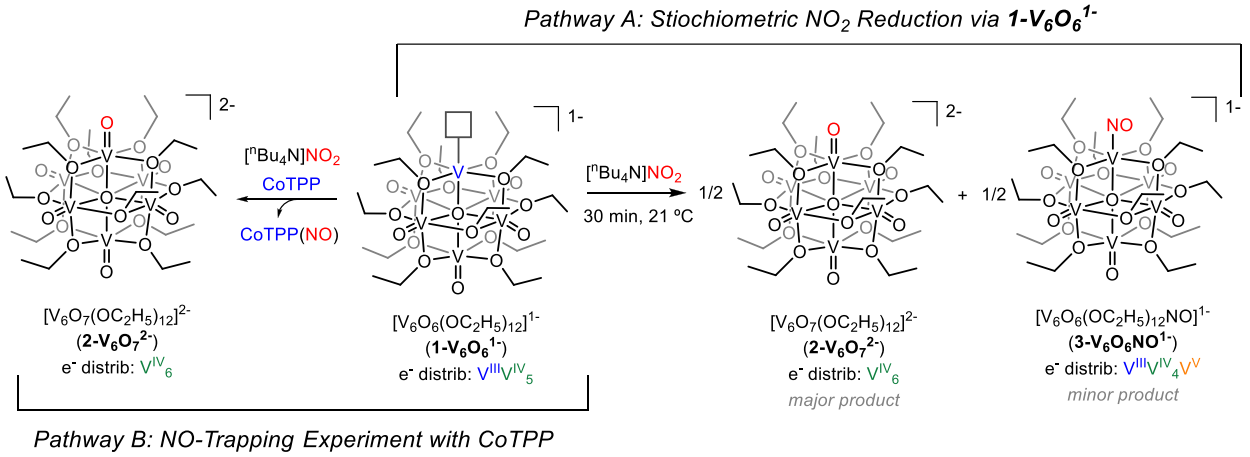

nitrate (NO_3^-). Analysis of the cluster-containing products reveals that all clusters, regardless of the oxidation state, are capable of mediating the one- and two-electron reduction of NO_2^- and NO_3^-, respectively. Insights into the factors that influence the rate of substrate activation are summarized, revealing the importance of surface ligands, ion-pairing interactions, and the distribution of oxidation states of remote vanadium ions in the OAT chemistry of these systems.

RESULTS AND DISCUSSION

Nitrite Reduction with $[CoCp_2][V_6O_6(OC_2H_5)_{12}]$. Previous work has demonstrated that an increased alkoxide chain length of the vanadium oxide assembly has no effect on the electronic structure of the hexavanadate core (Figure S1).[37,38] This suggests that similar OAT between nitrite and the anionic, monovacant POV-ethoxide cluster, $[V_6O_6(OC_2H_5)_{12}]^{1-}$ (**1-$V_6O_6^{1-}$**), might be observed. However, given that this ligand modification results in increased length of the bridging alkoxide ligands surrounding the active V^{III} ion, we anticipated discrepancies in the rate of the reaction, necessitating a series of control experiments to ascertain the consequences of the surface ligand identity on small molecule activation in these assemblies.

The addition of tetrabutylammonium nitrite ($[^nBu_4N]NO_2$, 1 equiv) to a red/brown solution of **1-$V_6O_6^{1-}$** in tetrahydrofuran resulted in the formation of a light-green suspension over the course of 30 min (Scheme 1, right). ^1H NMR analysis of the crude reaction mixture revealed consumption of the starting material and formation of a new product with signals consistent with those of the fully oxygenated POV-alkoxide cluster, $[V_6O_7(OC_2H_5)_{12}]^{2-}$ [**2-$V_6O_7^{2-}$**; $\delta(CD_3CN)$ = 26.5, −2.1 ppm; Figure S2].[31] Assignment of the oxidation state of the resulting POV-alkoxide was supported by cyclic voltammetry (CV) and open-circuit-potential measurements (Figure S3). However, spectroscopic characterization of the resulting reaction mixture via electronic absorption spectroscopy revealed the presence of intervalence charge-transfer (IVCT) bands located at 400 nm (ε = 5404 M^{-1} cm^{-1}) and 1000 nm (ε = 978 M^{-1} cm^{-1}), suggesting the formation of a *mixed-valent* POV-alkoxide (Figure S4).[39] This result is surprising given that the proposed product of this reaction, **2-$V_6O_7^{2-}$**, possesses an isovalent oxidation-state distribution of vanadium ions (V^{IV}_6).[30]

Perplexed by the apparent formation of a mixed-valent POV-alkoxide cluster, we reexamined the ^1H NMR spectrum of the crude reaction mixture (Figure S5). Small resonances were observed at 16.1 and −0.2 ppm, suggestive of the formation of an additional product. We hypothesized that this might be the result of product inhibition, where 1 equiv of nitric oxide, formed following NO_2^- reduction, binds to the oxygen-deficient vanadium(III) ion of unreacted **1-$V_6O_6^{1-}$**. Previous results from our laboratory have demonstrated that the coordination of nitric oxide to a site-differentiated POV-alkoxide cluster is facilitated by electron transfer from the reduced vanadium oxide scaffold, affording a net one-electron oxidation of the Lindqvist assembly.[40] When these results are translated to the current system, NO coordination would afford formation of the product-bound cluster $[V_6O_6NO(OC_2H_5)_{12}]^{1-}$ (**3-$V_6O_6NO^{1-}$**; Enemark−Feltham notation $\{VNO\}^3$), with an oxidized cluster core (ox. state distrib. = $V^{III}V^{IV}_4V^V$), justifying the observed IVCT bands in the absorption spectrum.

To probe this hypothesis, a substoichiometric amount of NO_2^- (0.5 equiv) was added to complex **1-$V_6O_6^{1-}$**. ^1H NMR analysis of the crude reaction mixture showed complete conversion of the starting material and growth of resonances consistent with formation of the oxygenated POV-alkoxide cluster and those tentatively assigned to **3-$V_6O_6NO^{1-}$** [$\delta(CD_3CN)$ = 16.4, −0.2 ppm; Figure S6]. Electrospray ionization mass spectrometry [ESI-MS; (−)mode] revealed two main signals (m/z 958 and 972; Figure S7). The first (m/z 958) corresponds to the fully oxygenated Lindqvist cluster and is consistent with the resonances observed in the ^1H NMR spectra at 26.7 and −2.0 ppm. The signal at m/z 972 is consistent with the molecular weight of the NO-bound POV-alkoxide, **3-$V_6O_6NO^{1-}$**. Further support for formation of the NO adduct was obtained through IR spectroscopy; a transition centered at 1537 cm^{-1} was observed, resembling values previously reported for vanadium complexes with a nitric oxide ligand (Figure S8).[41,42]

We hypothesized that NO removal from the crude reaction mixture, via the addition of a NO-trapping agent [e.g., cobalt(II) tetraphenylporphyrin, CoTPP], should disfavor the formation of complex **3-$V_6O_6NO^{1-}$**.[43−45] Therefore, NO_2^- was added to a mixture of **1-$V_6O_6^{1-}$** and CoTPP and analyzed by electronic absorption spectroscopy (Figure 2; see Figure S9

https://dx.doi.org/10.1021/acs.inorgchem.0c02052
Inorg. Chem. 2021, 60, 6855−6864

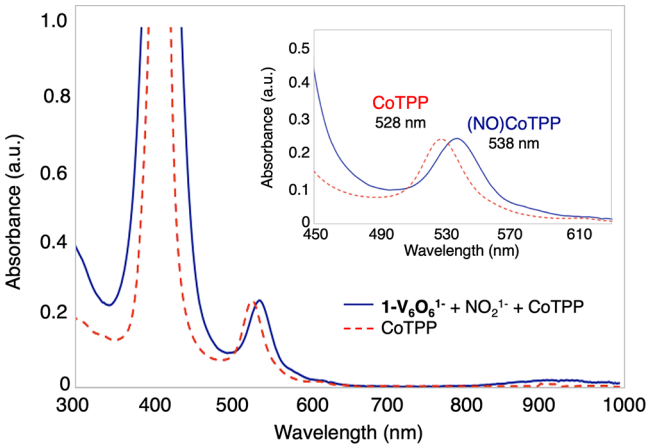

Figure 2. Electronic absorption spectra of CoTPP (red, dotted) and the NO-trapping experiment featuring the in situ reaction of CoTPP, **1-$V_6O_6^{1-}$**, and NO_2^- (blue). The blue spectrum reveals that the lower-energy region (λ = 1000 nm) lacks IVCT bands. The figure inset shows the shift in the Q band of the cobalt porphyrin complex, consistent with the quantitative formation of (NO)CoTPP. Absorption spectra are collected in dichloromethane at 21 °C.

for control experiments). Investigation of the change in energy of the Q band of the CoTPP complex revealed the expected diagnostic shift from 528 to 538 nm, consistent with quantitative conversion of NO_2^- to NO [i.e., the quantitative formation of (NO)CoTPP; Figure 2, inset; see the Experimental Section for more details]. The lack of an IVCT band at ∼1000 nm in the absorption spectra confirms sole formation of the isovalent Lindqvist cluster, **2-$V_6O_7^{2-}$** (Figure 2 and Scheme 1, left). This is further confirmed by ^{1}H NMR analysis, which shows no evidence of formation of the mixed-valent byproduct, **3-$V_6O_6NO^{1-}$** (Figure S10).

At face value, the discrepancy in the product distribution following nitrite activation between the oxygen-deficient POV-methoxide and -ethoxide clusters is surprising, given their similar electronic properties and reduction potential (Figure S1).[37,38] However, justification for this observation can be made through consideration of the consequences of increased steric bulk at the site-differentiated vanadium(III) center. We hypothesize that coordination of nitric oxide is observed in the case of the ethoxide cluster because of the fact that the association of a solvent, tetrahydrofuran, to the vacant site is disfavored as a result of the bulk of the ethoxide ligands. Indeed, a decreased binding affinity of bulky substrates to the reduced vanadium center in oxygen-deficient POV-*ethoxide* clusters has been reported previously by our group.[32] The poor association between the solvent and oxygen-deficient POV-alkoxide cluster results in the formation of a coordinatively unsaturated vanadium(III) center, lowering the activation barrier for the formation of complex **3-$V_6O_6NO^{1-}$**. Similarly, the increased steric bulk of the alkoxide ligands also explains the variation in the reaction rate between the ethoxide- and methoxide-bridged clusters [**1-$V_6O_6^{1-}$** (30 min); $[V_6O_6(OCH_3)_{12}]^{1-}$ (24 h), Table 1].[30] Increased access to the vanadium(III) ion, in the case of the ethoxide-bridged derivative, enhances the overall rate of the reaction by eliminating the kinetically inhibiting step of solvent dissociation from the reaction pathway.

Assessing the Charge State Dependence of POV-alkoxide Clusters in Nitrite Reduction. Interested in analyzing the sensitivity of substrate activation toward the

Table 1. Comparative Reaction Times and Temperatures for NO_2^- Reduction via $[V_6O_6(OCH_3)_{12}]^{1-}$,[38] 1-$V_6O_6^{1-}$, 4-$V_6O_6^0$, and 6-$V_6O_6^{1+}$

complex	oxidation state distribution	NO_2^- reduction reaction conditions	open-circuit-potential for the NO_2^- reduction reaction[a]
$[V_6O_6(OCH_3)_{12}]^{1-}$	$V^{III}V^{IV}_5$	24 h, 21 °C	
1-$V_6O_6^{1-}$	$V^{III}V^{IV}_5$	30 min, 21 °C	−1.14
4-$V_6O_6^0$	$V^{III}V^{IV}_4V^{V}$	5 min, 21 °C	−0.65
6-$V_6O_6^{1+}$	$V^{III}V^{IV}_3V^{V}_2$	15 min, 21 °C	−0.51

[a]Open-circuit-potential listed in volts versus $Fc^{0/+}$ in dichloromethane. See Figures S3, S14, and S18 for cyclic voltammograms of NO_2^- reduction via **1-$V_6O_6^{1-}$**, **4-$V_6O_6^0$**, and **6-$V_6O_6^{1+}$**, respectively.

charge state of the Lindqvist cluster, we sought to investigate NO_2^- reduction with the neutral, oxygen-deficient POV-ethoxide cluster $[V_6O_6(OC_2H_5)_{12}]^0$ (**4-$V_6O_6^0$**). The addition of 1 equiv of NO_2^- to **4-$V_6O_6^0$** in tetrahydrofuran resulted in an immediate color change from brown to green at 21 °C. Analysis of an aliquot of the crude reaction mixture by ^{1}H NMR spectroscopy revealed complete conversion to a product with two resonances located at 25.8 and −1.9 ppm after only 5 min (Figure S11; see Figures S12−S15 for full characterization of the product **5-$V_6O_7^{1-}$**). Notably, no additional resonances corresponding to an NO-ligated species were observed in this spectrum. This is likely due to the oxidized nature of complex **4-$V_6O_6^0$**, which inhibits electron transfer from the vanadium oxide cluster to nitric oxide.[46]

To complete analysis of NO_2^- reduction with the redox series of POV-ethoxide clusters, we explored NO_2^- activation with the cationic, monovacant, POV-ethoxide cluster $[V_6O_6(OC_2H_5)_{12}]^{1+}$ (**6-$V_6O_6^{1+}$**).[35] As expected, the addition of NO_2^- to a solution of **6-$V_6O_6^{1+}$** results in the quantitative formation of NO and $[V_6O_7(OC_2H_5)_{12}]^0$ (**7-$V_6O_7^0$**; Figures S16−S20). OAT from the substrate to the cationic oxygen-deficient cluster was rapid, reaching completion after 15 min.

While the rates of NO_2^- reduction for all charge states of the ethoxide-bridged clusters are significantly increased in comparison to that reported for $[V_6O_6(OCH_3)_{12}]^{1-}$, the discrepancies in the reaction time between **1-$V_6O_6^{1-}$** and the more oxidized clusters (i.e., **4-$V_6O_6^0$** and **6-$V_6O_6^{1+}$**) confirms that the charge state of the POV-alkoxide assembly influences substrate activation (Table 1). To rationalize these observations, we considered the repulsive, anion−anion interactions between complex **1-$V_6O_6^{1-}$** and NO_2^-. These electrostatic contributions likely influence substrate coordination to the oxygen-deficient vanadium(III) center, resulting in a higher activation barrier for this binding event, which manifests in a longer reaction time. In contrast, the neutral and cationic POV-ethoxide clusters do not experience these repulsive ion-pairing interactions. This translates to more rapid OAT chemistry for these clusters compared to that of **1-$V_6O_6^{1-}$**. Similar influences on the reaction rates resulting from ion-pairing interactions have been reported for monometallic transition metal complexes.[47−50]

While the repulsive ion-pairing interactions offer an explanation for the increased reaction time required for NO_2^- reduction via the anionic cluster, this theory would suggest that the cationic species would have the fastest rate of substrate reduction (attractive ion-pairing interactions with the oxyanion). However, a comparison of the reaction time for NO_2^- reduction between the neutral and cationic species

https://dx.doi.org/10.1021/acs.inorgchem.0c02052
Inorg. Chem. 2021, 60, 6855−6864

Scheme 2. Addition of NO_3^- to 4-$V_6O_6^0$ Resulting in the Formation of an NO-Bound Species, 8-$V_6O_6NO_3^{1-}$ (Middle), Which Converts to the Fully Oxygenated Cluster after Stirring in Tetrahydrofuran at 50 °C (Right)[a]

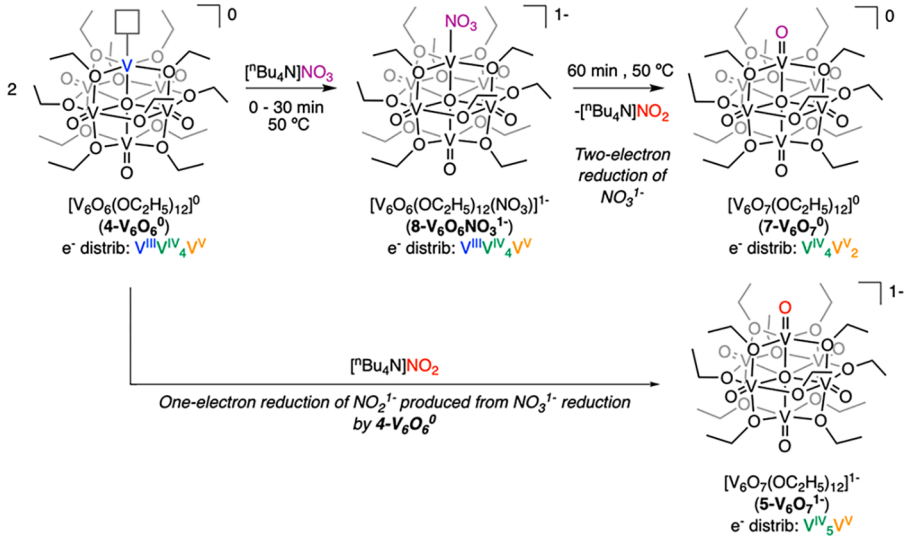

[a]See Figure 3 for the ^{1}H NMR spectra.

reveals that a 3-fold increase in the reaction time is required for N−O bond scission (Table 1). The discrepancy in the reaction rates of nitrite deoxygenation by the neutral and cationic oxygen-deficient POV-alkoxide clusters suggests that the oxidation state of remote transition metal ions within the POV-alkoxide cluster plays a role in substrate activation. Indeed, previous analysis of the oxidation state of vanadyl ions embedded within oxygen-deficient POV-alkoxides, $[V_6O_6(OR)_{12}]^n$, has shown that the redox chemistry of these clusters is localized to the Lindqvist core (e.g., e^- distrib. **1-$V_6O_6^{1-}$** = $V^{III}V^{IV}_5$; e^- distrib. **4-$V_6O_6^0$** = $V^{III}V^{IV}_4V^V$; e^- distrib. **6-$V_6O_6^{1+}$** = $V^{III}V^{IV}_3V^V_2$).

Similar effects of changing the oxidation state of remote transition metal ions within multimetallic inorganic complexes on the reactivity of these assemblies have been reported previously.[51−56] For example, Agapie and co-workers reported the synthesis and characterization of a set of iron−manganese clusters, $[Fe_3Mn]^n$ (n = 2+, 3+).[51] Electronic characterization of these molecules revealed that the one-electron reduction of the cluster is localized to the triiron base of the assembly (i.e., $[Fe^{III}_3Mn^{II}] \rightarrow [Fe^{II}Fe^{III}_2Mn^{II}]$), with the site-differentiated manganese ion retaining its 2+ oxidation state. Upon the introduction of an oxidant, the authors noticed pronounced differences in the reactivity of the two complexes; the more oxidized cluster exhibited a 100-fold decreased in the reaction time in comparison to that of the reduced derivative. Given that the transition metal directly participating in OAT, namely, the site-differentiated manganese ion, possesses a 2+ oxidation state in both the reduced and oxidized variants, the authors attribute the differences in the reaction time to the influence of changes in the oxidation states of remote transition metal ions. Subsequent investigations confirm that the rate of OAT, activation parameters, and M−OR bond dissociation energies are significantly influenced by variation of the charge state of the basal iron centers in these multimetallic systems.[52−54,56]

Assessing the Charge State Dependence of POV-alkoxide Clusters in Nitrate Reduction. With new insights into the factors that dictate the rate of OAT from nitrite to oxygen-deficient POV-alkoxide clusters in hand, we shifted our focus toward extending these investigations to nitrate (NO_3^-) reduction. The two-electron reduction of NO_3^- is considerably more endergonic, requiring more than double the energy to facilitate substrate activation ($\Delta G_{NO_3-NO_2}$ = ∼20 kcal mol^{-1};[57] ΔG_{NO_2-NO} = ∼8 kcal mol^{-1}).[58] Given the increased thermodynamic stability of NO_3^-, we hypothesized that OAT would be more drastically influenced by variation of the redox potential of the cluster, likely resulting in a significantly increased reaction time with more electron-deficient assemblies.

In our initial study describing NO_x^- activation by oxygen-deficient POV-alkoxide clusters, we reported that the addition of tetrabutylammonium nitrate ($[^nBu_4N]NO_3$) to $[V_6O_6(OCH_3)_{12}]^{1-}$ resulted in reduction to nitric oxide via the following series of reactions: (1) the two-electron reduction of NO_3^- results in N−O bond cleavage and the formation of NO_2^- and the fully oxygenated POV-alkoxide cluster in the monoanionic charge state $[V_6O_7(OCH_3)_{12}]^{1-}$ (eq 1) and (2) the NO_2^- generated in situ rapidly reacts with an additional 1 equiv of oxygen-deficient POV-alkoxide, resulting in the formation of NO and the dianionic vanadium oxide cluster $[V_6O_7(OCH_3)_{12}]^{2-}$ (eq 2).[30] Overall, the reduction of nitrate affords a mixture of vanadium-containing products in a 1:1 ratio, namely, $[V_6O_7(OCH_3)_{12}]^{1-}$ and $[V_6O_7(OCH_3)_{12}]^{2-}$ (eq 3).

$$2[V_6O_6(OR)_{12}]^{1-} + NO_3^- \rightarrow [\mathbf{V_6O_7(OR)_{12}}]^{1-} + NO_2^- + [V_6O_6(OR)_{12}]^{1-} \quad (1)$$

$$[V_6O_6(OR)_{12}]^{1-} + NO_2^- \rightarrow [\mathbf{V_6O_7(OR)_{12}}]^{2-} + \mathbf{NO} \quad (2)$$

$$2[V_6O_6(OR)_{12}]^{1-} + NO_3^- \rightarrow [\mathbf{V_6O_7(OR)_{12}}]^{2-} + [\mathbf{V_6O_7(OR)_{12}}]^{1-} + \mathbf{NO} \quad (3)$$

Given that the one-electron reduction of NO_2^- resulted in the same net transformation for both the methoxide- and ethoxide-bridged clusters, we hypothesized that the reduction of NO_3^- mediated by **1-$V_6O_6^{1-}$** would result in the formation

https://dx.doi.org/10.1021/acs.inorgchem.0c02052
Inorg. Chem. 2021, 60, 6855−6864

of an analogous mixture of cluster-containing products. Optimization of the reaction conditions revealed that heating a solution of $[^nBu_4N]NO_3$ (1 equiv) and complex **1-$V_6O_6^{1-}$** at 50 °C for 24 h results in complete conversion of the starting material (Figure S21). Spectroscopic analysis of the cluster-containing products revealed that the reduction of NO_3^- by **1-$V_6O_6^{1-}$** resulted in the expected product mixture of the anionic cluster (**5-$V_6O_7^{1-}$**, formed from the two-electron reduction of NO_3^-) and dianionic cluster (**2-$V_6O_7^{2-}$**, formed from the one-electron reduction of NO_2^-; Figures S22–S24).

To elucidate the consequences of the cluster charge state on the two-electron reduction of NO_3^-, we next attempted NO_3^- activation with the neutral, monovacant cluster (**4-$V_6O_6^0$**). ^{1}H NMR analysis revealed complete conversion of the oxygen-deficient assembly after 1.5 h (Figure S25; see Figures S26–S28 for full characterization). However, analysis of aliquots taken at earlier time points (t = 0–30 min) revealed the formation of a new paramagnetic product [$\delta(CDCl_3)$ = 28.7, 22.4, −0.5, −2.4, and −23.7 ppm; Scheme 2 and Figure 3].

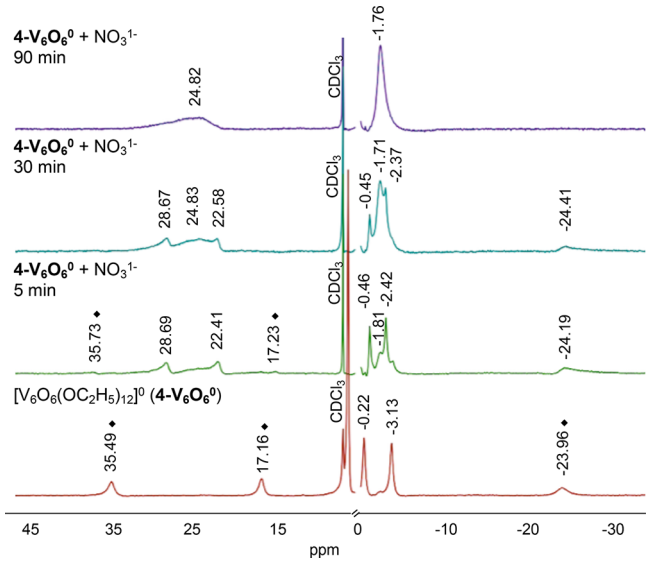

Figure 3. ^{1}H NMR spectra of the reaction of **4-$V_6O_6^0$** and $[^nBu_4N]NO_3$ over the course of 90 min at 50 °C in $CDCl_3$. NMR reveals that NO_3^- addition to the neutral cluster results in the immediate formation of complex **8-$V_6O_6NO_3^{1-}$** (green), which converts to the fully oxygenated clusters (purple). Resonances attributed to **4-$V_6O_6^0$** are labeled with "◆". Slight shifts of the paramagnetic resonances of **4-$V_6O_6^0$** are observed at t = 5 min (green spectrum), likely due to fluctional solvent coordination.

Previous reports from our laboratory analyzing ligand coordination to oxygen-deficient POV-alkoxide clusters revealed that the addition of weakly coordinated anions,[31] halogens,[35,36] or phosphine oxides[32] (i.e., −OTf, −Cl, $-OPR_3$) to the unsaturated vanadium(III) ion embedded within the reduced POV-ethoxide assembly results in a five-peak pattern in the ^{1}H NMR spectra. Thus, we hypothesized that these resonances correspond to a nitrate-bound POV-ethoxide intermediate, $[V_6O_6(OC_2H_5)_{12}(NO_3)]^{1-}$ (**8-$V_6O_6(NO_3)^{1-}$**).

Further evidence supporting the formation of **8-$V_6O_6(NO_3)^{1-}$** was obtained by ESI-MS and IR spectroscopy. The ESI-MS spectrum of **8-$V_6O_6(NO_3)^{1-}$** contained two prominent signals with mass-to-charge (m/z) ratios of 958 and 1004 [(−)mode; Figure S29]. The signal with m/z 958 corresponds to the fully oxygenated POV-ethoxide cluster $[V_6O_7(OC_2H_5)_{12}]^n$ and likely results from the instability of complex **8-$V_6O_6(NO_3)^{1-}$** under ESI-MS conditions. The remaining signal is consistent with the molecular mass of the monovacant cluster (**4-$V_6O_6^0$**) plus an equivalent of NO_3^- (m/z 1004). Furthermore, the IR spectra of complex **8-$V_6O_6(NO_3)^{1-}$** contained the expected stretching frequencies associated with vanadyl moieties within the Lindqvist scaffold (1049 and 953 cm^{-1}) as well as additional features ranging from 1330 to 1462 cm^{-1}, which are similar to the NO_3^- vibrational modes in the IR spectra of nitrate-bound transition metal complexes (Figure S30).[59,60] Unfortunately, attempts to crystallize complex **8-$V_6O_6(NO_3)^{1-}$** were thwarted by its instability; complex **8-$V_6O_6(NO_3)^{1-}$** readily converts to the fully oxygenated POV-ethoxide clusters (**5-$V_6O_7^{1-}$** and **7-$V_6O_7^0$**; Figure S31) in solution at room temperature. This conversion supports that NO_3^- reduction with the POV-alkoxide clusters follows a Mars–van Krevelen-type mechanism; coordination of nitrate to the site-differentiated vanadium(III) ion embedded within the reduced Lindqvist cluster leads to substrate reduction, N–O bond cleavage, and, ultimately, OAT.

Table 2. Comparative Reaction Times and Temperatures for NO_3^- Reduction via $[V_6O_6(OCH_3)_{12}]^{1-}$,[38] 1-$V_6O_6^{1-}$, 4-$V_6O_6^0$, and 6-$V_6O_6^{1+}$

complex	oxidation state distribution	NO_3^-reduction reaction conditions	open-circuit-potential for the NO_3^- reduction reaction[a]
$[V_6O_6(OCH_3)_{12}]^{1-}$	$V^{III}V^{IV}_5$	24 h, 70 °C[a]	
1-$V_6O_6^{1-}$	$V^{III}V^{IV}_5$	24 h, 50 °C	−1.08
4-$V_6O_6^0$	$V^{III}V^{IV}_4V^{V}$	1.5 h, 50 °C	−0.59
6-$V_6O_6^{1+}$	$V^{III}V^{IV}_3V^{V}_2$	96 h, 50 °C	−0.24

[a]A direct comparison of nitrate reduction by the POV-ethoxide and -methoxide clusters can be found in Figures S36 and S37. [b]OCP listed in volts versus $Fc^{0/+}$ in dichloromethane. See Figures S24, S28, and S35 for cyclic voltammograms of NO_3^- reduction via **1-$V_6O_6^{1-}$**, **4-$V_6O_6^0$**, and **6-$V_6O_6^{1+}$**, respectively.

To complete our investigations of nitrate reduction with the redox series of oxygen-deficient POV-alkoxide clusters, we next investigated the reactivity of complex **6-$V_6O_6^{1+}$** with $[^nBu_4N]$-NO_3. To our surprise, the reaction took 96 h to reach completion—substantially longer than its anionic and neutral congeners (Table 2; see Figures S32–S35 for product characterization). These results provide unambiguous evidence that the charge state of remote vanadyl ions within the POV-alkoxide assembly influences substrate activation. Indeed, although the site-differentiated vanadium(III) ion, which is retained throughout all charge states, directly participates in OAT, the overall electron-deficient nature of the hexavanadate core of complex **6-$V_6O_6^{1+}$** (e^- distrib. $V^{III}V^{IV}_3V^{V}_2$) impedes electron transfer to nitrate, inhibiting the rate of N–O bond cleavage and resulting in a significant increase in the reaction time.

The relative influence of ion-pairing interactions and the cluster redox potential can be compared by analyzing the reaction time required for NO_3^- reduction by the anionic and cationic clusters, respectively (Table 2). These results reveal that while repulsive ion-pairing interactions certainly inhibit substrate deoxygenation (**1-$V_6O_6^{1-}$** vs **4-$V_6O_6^0$**; 16-fold increase in the reaction time due to ion pairing), in the case of nitrate reduction, the electronics of the metal oxide cluster

https://dx.doi.org/10.1021/acs.inorgchem.0c02052
Inorg. Chem. 2021, 60, 6855–6864

has a more substantial effect on the rate of substrate activation (**6-$V_6O_6^{1+}$** vs **4-$V_6O_6^{0}$**; 64-fold increase in the reaction time due to the redox potential). Overall, these investigations confirm that remote redox changes within the metal oxide assembly play a significant role in the surface activity of these materials.

CONCLUSION

In this work, we have demonstrated that NO_x^- (x = 2, 3) reduction is significantly influenced by the charge state of oxygen-deficient POV-alkoxide clusters. While the oxidation state of remote vanadyl ions clearly plays a role in dictating the rate and extent to which OAT reactions proceed, our investigations have revealed that two additional factors can influence OAT with these polynuclear assemblies: (1) the steric bulk imparted on the active metal center by surrounding surface ligands and (2) electrostatic interactions between the substrate and cluster. The former is evident in comparing the reaction time required for oxyanion reduction via complex **1-$V_6O_6^{1-}$** to that of the anionic, methoxide-bridged POV-alkoxide cluster, ($[V_6O_6(OCH_3)_{12}]^{1-}$), which reveals that increasing the steric bulk results in enhanced oxyanion coordination. Similarly, the dramatic increase of the reaction time required for NO_2^- reduction in the case of the monoanionic POV-alkoxide cluster (**1-$V_6O_6^{1-}$**), relative to that of the neutral and cationic species, reveals that electrostatic repulsion between the most-reduced cluster and substrate significantly influences the rate of OAT. The factors that have emerged from our structure–function investigations reveal design strategies that might improve the reactivity of metal oxide materials in small-molecule activation schematics. Future work analyzing OAT chemistry with these reduced, vanadium oxide assemblies will focus on the study of OAT from *neutral* substrates in order to decouple the influence of ion-pairing interactions from that of the change in the remote metal oxidation state.

EXPERIMENTAL SECTION

General Considerations. All manipulations were carried out in the absence of water and dioxygen using standard Schlenk techniques or in a UniLab MBraun inert-atmosphere drybox under a dinitrogen atmosphere except where specified otherwise. All glassware was oven-dried for a minimum of 3 h and cooled in an evacuated antechamber prior to use in the drybox. All solvents were dried and deoxygenated on a Glass Contour System (Pure Process Technology, LLC) and stored over activated 3 Å molecular sieves purchased from Fisher Scientific prior to use. $[CoCp_2]V_6O_6(OC_2H_5)_{12}$ (**1-$V_6O_6^{1-}$**),[34] $[V_6O_6(OC_2H_5)_{12}]^0$ (**4-$V_6O_6^{0}$**),[32] and $[V_6O_6(OC_2H_5)_{12}]^{1+}$ (**6-$V_6O_6^{1+}$**)[33] were prepared according to previously published procedures. Tetrabutylammonium nitrite and nitrate were purchased from Sigma-Aldrich and stored in the drybox over P_2O_5. 5,10,15,20-Tetraphenyl-21*H*,23*H*-porphinecobalt(II) (CoTPP), silver triflate, and cobaltocene ($CoCp_2$) were purchased from Sigma-Aldrich and used as received.

All ^{1}H NMR spectra were recorded at 400 MHz on a Bruker DPX-400 MHz spectrometer locked on the signal of deuterated solvents. All chemical shifts were reported relative to the peak of a residual H signal in deuterated solvents. Acetonitrile (CD_3CN) and chloroform ($CDCl_3$) were purchased from Cambridge Isotope Laboratories, degassed by three freeze–pump–thaw cycles, and stored in the drybox over activated 3 Å molecular sieves. IR (Fourier transform and attenuated total relectance) spectra of complexes were recorded on a Shimadzu IRAffinity-1 Fourier transform infrared spectrophotometer and are reported in wavenumbers (cm^{-1}). Electronic absorption measurements were recorded at room temperature in anhydrous dichloromethane in a sealed 1 cm quartz cuvette with an Agilent Cary 60 UV–vis spectrophotometer. CV experiments were recorded with a Bio-Logic SP200 potentiostat/galvanostat and the *EC-Lab* software suite. All measurements were performed in a three-electrode system cell configuration that consisted of a glassy carbon (ø = 3.0 mm) as the working electrode (CH Instruments, USA), platinum wire as the counter electrode (CH Instruments, USA), and Ag/Ag^+ as the nonaqueous reference electrode with 0.01 M $AgNO_3$ in 0.05 M $[^nBu_4N][PF_6]$ in dichloromethane (BASi, USA). All electrochemical measurements were performed at room temperature in a dinitrogen-filled drybox. Anhydrous dichloromethane (DCM) that contained $[^nBu_4N][PF_6]$ was used as the electrolyte solution.

Capture of Nitric Oxide by CoTPP. To probe whether nitric oxide was produced in nitrite reduction with $[V_6O_6(OC_2H_5)_{12}]^n$ (n = 1−, 0, 1+), CoTPP was added to the reaction mixture. CoTPP, a NO complexation agent, exhibits a highly characteristic shift in the position of the absorption band ($\lambda_{CoTPP,initial}$ = 528 nm in dichloromethane) following NO coordination.[43−45,61] A calibration curve, collected in dichloromethane by Symes and co-workers, was used to qualitatively measure the amount of NO-ligated CoTPP formed.[43] ^{1}H NMR measurements were taken in $CDCl_3$ to further assess (NO)CoTPP formation via the growth of new resonances at 8.91, 8.17, and 7.74 ppm, which match the previously reported spectra for the NO-ligated CoTPP complex.[61] Control experiments: Six 20 mL scintillation vials were charged with (1) CoTPP and **1-$V_6O_6^{1-}$**, (2) CoTPP and **4-$V_6O_6^{0}$**, (3) CoTPP and **6-$V_6O_6^{1+}$**, (4) CoTPP and **5-$V_6O_7^{1-}$**, (5) CoTPP and **7-$V_6O_6^{0}$**, and (6) CoTPP and **9-$V_6O_7^{1+}$** each in 6 mL of tetrahydrofuran. The reactions mixtures were stirred for 24 h at 21 and 50 °C, after which 0.01 mL was removed and diluted with 10 mL anhydrous dichloromethane. Electronic absorbance spectroscopy was used to measure the initial absorbance band of CoTPP and that of each reaction mixture (Figure S9).

General Reaction Procedure for NO Trapping Using CoTPP. In a glovebox, a 20 mL scintillation vial or 15 mL pressure vessel was charged with $[V_6O_6(OC_2H_5)_{12}]^n$ (n = −1, 0, 1+) and 8 mL of tetrahydrofuran. CoTPP (1 equiv) and $[^nBu_4N]NO_2$ (1 equiv) were added to the solution as solids. The reaction mixture was stirred at (1) 21 °C for 24 h (**1-$V_6O_6^{1-}$**), (2) 50 °C for 24 h (**4-$V_6O_6^{0}$**), and (3) 50 °C for 24 h (**6-$V_6O_6^{1+}$**), after which 0.01 mL was removed from the reaction mixture and diluted with 10 mL of anhydrous dichloromethane. Electronic absorbance spectroscopy was used to measure the shift in the wavelength following NO complexation to CoTPP ($\lambda_{CoTPP,initial}$ = 528 nm in dichloromethane).

(1) **1-$V_6O_6^{1-}$** + $[^nBu_4N]NO_2$. **1-$V_6O_6^{1-}$** (0.010 g, 0.009 mol), CoTPP (0.006 g, 0.009 mol), and $[^nBu_4N]NO_2$ (0.003 g, 0.009 mol). ^{1}H NMR (400 MHz, $CDCl_3$): δ 27.24 (fwhh = 466 Hz), 8.91 (fwhh = 32 Hz), 8.17 (fwhh = 40 Hz), 7.74 (fwhh = 40 Hz), −1.91 (fwhh = 224 Hz). UV–vis (CH_2Cl_2): 538 nm.

(2) **4-$V_6O_6^{0}$** + $[^nBu_4N]NO_2$. **4-$V_6O_6^{0}$** (0.028 g, 0.029 mol), CoTPP (0.019 g, 0.029 mol), and $[^nBu_4N]NO_2$ (0.008 g, 0.029 mol). ^{1}H NMR (400 MHz, $CDCl_3$): δ 26.81 (fwhh = 1364 Hz), 15.93 (fwhh = 108 Hz), 13.14 (fwhh = 80 Hz), 9.94 (fwhh = 32 Hz), 9.74 (fwhh = 32 Hz), 8.91 (fwhh = 20 Hz), 8.17 (fwhh = 28 Hz), 7.74 (fwhh = 28 Hz), −2.09 (fwhh = 432 Hz). UV–vis (CH_2Cl_2): 538 nm.

(3) **6-$V_6O_6^{1+}$** + $[^nBu_4N]NO_2$. **6-$V_6O_6^{1+}$** (0.019 g, 0.017 mol), CoTPP (0.012 g, 0.018 mol), and $[^nBu_4N]NO_2$ (0.005 g, 0.018 mol). ^{1}H NMR (400 MHz, $CDCl_3$): δ 23.98 (fwhh = 1252 Hz), 8.91 (fwhh = 20 Hz), 8.17 (fwhh = 528 Hz), 7.74 (fwhh = 24 Hz), −1.64 (fwhh = 328 Hz). UV–vis (CH_2Cl_2): 538 nm.

Nitrite Reduction with $[CoCp_2][V_6O_6(OC_2H_5)_{12}]$ (1-$V_6O_6^{1-}$). In a glovebox, a 20 mL scintillation vial was charged with **1-$V_6O_6^{1-}$** (0.010 g, 0.009 mmol) and 8 mL of tetrahydrofuran. $[^nBu_4N]NO_2$ (0.003 g, 0.009 mmol, 1 equiv) was added to the solution as a solid. The reaction mixture was stirred for 30 min at 21 °C, after which the volatiles were removed under vacuum to yield a mixture of **2-$V_6O_7^{2-}$** and **3-$V_6O_6NO^{1-}$**. ^{1}H NMR (400 MHz, CD_3CN): δ 26.47 (**2-$V_6O_7^{2-}$**; fwhh = 928 Hz), 16.10 (**3-$V_6O_6NO^{1-}$**; fwhh = 352 Hz), 5.66 (fwhh = 56 Hz), 3.06 (fwhh = 68 Hz), 1.58, 1.33, 0.96, −0.20 (**3-$V_6O_6NO^{1-}$**; fwhh = 132 Hz), −2.05 (**2-$V_6O_7^{2-}$**; fwhh = 260 Hz). FT-IR (ATR, cm^{-1}): 1053 (O–C_2H_5), 932 (V=O). UV–vis (CH_2Cl_2):

https://dx.doi.org/10.1021/acs.inorgchem.0c02052
Inorg. Chem. 2021, 60, 6855−6864

400 nm (ε = 5404 M^{-1} cm^{-1}), 1000 nm (ε = 978 M^{-1} cm^{-1}). Note: The molar absorptivity was calculated as if the product was a dianionic cluster (MW = 1389.95).

Substoichiometric Nitrite Reduction with $[CoCp_2][V_6O_6(OC_2H_5)_{12}]$ ($1\text{-}V_6O_6^{1-}$). In a glovebox, a 20 mL scintillation vial was charged with $1\text{-}V_6O_6^{1-}$ (0.037 g, 0.033 mmol) and 20 mL of tetrahydrofuran. $[^nBu_4N]NO_2$ (0.005 g, 0.016 mmol, 0.48 equiv) was added to the solution as a solid. The reaction mixture was stirred for 24 h at 21 °C, after which the volatiles were removed under vacuum to yield a mixture of $2\text{-}V_6O_7^{2-}$ and $3\text{-}V_6O_6NO^{1-}$. ^{1}H NMR (400 MHz, CD_3CN): δ 26.49 ($2\text{-}V_6O_7^{2-}$; fwhh = 756 Hz), 16.35 ($3\text{-}V_6O_6NO^{1-}$; fwhh = 720 Hz), 5.68 (fwhh = 40 Hz), 3.06 (fwhh = 28 Hz), 1.59, 1.34, 0.96, −0.14 ($3\text{-}V_6O_6NO^{1-}$; fwhh = 192 Hz), −2.02 ($2\text{-}V_6O_7^{2-}$; fwhh = 280 Hz). FT-IR (ATR, cm^{-1}): 1535 (NO), 1045 (O−C_2H_5), 937 (V═O). UV−vis (CH_2Cl_2): 398 nm (ε = 2778 M^{-1} cm^{-1}), 1000 nm (ε = 487 M^{-1} cm^{-1}). Note: The molar absorptivity was calculated as if the product was a dianionic cluster (MW = 1389.95).

Nitrite Reduction with $V_6O_6(OC_2H_5)_{12}(CH_3CN)$ ($4\text{-}V_6O_6^0$). In a glovebox, a 20 mL scintillation vial was charged with $4\text{-}V_6O_6^0$ (0.040 g, 0.041 mmol) and 8 mL of tetrahydrofuran. $[^nBu_4N]NO_2$ (0.012 g, 0.041 mmol, 1 equiv) was added to the solution as a solid. The reaction mixture was stirred for 5 min at 21 °C, after which the crude reaction mixture was filtered and the volatiles were removed under vacuum to yield $5\text{-}V_6O_7^{1-}$ (0.028 g, 0.023 mmol, 92%). Analytical data obtained for complex $5\text{-}V_6O_7^{1-}$ via standard characterization techniques matched those obtained from previously reported syntheses.[38,39]

Synthesis of $[V_6O_6(OC_2H_5)_{12}]$OTf ($6\text{-}V_6O_6^{1+}$). The synthesis of $6\text{-}V_6O_6^{1+}$ was adapted from a previous report.[35] In a glovebox, a 20 mL scintillation vial was charged with $4\text{-}V_6O_6^0$ (0.056 g, 0.057 mmol) and 8 mL of dichloromethane. Silver trifluoromethylsulfonate (0.018 g, 0.070 mmol, 1.2 equiv) was added to the solution as a solid. The reaction mixture was stirred for 2 h at 21 °C, after which the product was filtered and the volatiles were removed under vacuum to yield $6\text{-}V_6O_6^{1+}$ (0.056 g, 0.052 mmol, 90%). Analytical data obtained for complex $6\text{-}V_6O_6^{1+}$ via standard characterization techniques (^{1}H NMR, IR, and UV−vis) matched those obtained from a previously reported synthesis.[35]

Nitrite Reduction with $V_6O_6(OC_2H_5)_{12}$OTf ($6\text{-}V_6O_6^{1+}$). In a glovebox, a 20 mL scintillation vial was charged with $6\text{-}V_6O_6^{1+}$ (0.023 g, 0.021 mmol) and 8 mL of tetrahydrofuran. $[^nBu_4N]NO_2$ (0.006 g, 0.021 mmol, 1 equiv) was added to the solution as a solid. The reaction mixture was stirred for 15 min at 21 °C, after which the product was filtered and the volatiles were removed under vacuum to yield a mixture of $7\text{-}V_6O_7^0$ and $[^nBu_4N]$OTf (0.044 g, 0.033 mmol, 83%). Note: The yield was calculated assuming that the product contains a 1:1 ratio of the cluster-containing product and salt (MW = 1349.90). Analytical data obtained for $7\text{-}V_6O_7^0$ via standard characterization techniques matched those obtained from previously reported syntheses.[38,39]

Nitrate Reduction with $[CoCp_2][V_6O_6(OC_2H_5)_{12}]$ ($1\text{-}V_6O_6^{1-}$). In a glovebox, a 20 mL scintillation vial was charged with $1\text{-}V_6O_6^{1-}$ (0.019 g, 0.017 mmol) and 8 mL of tetrahydrofuran. $[^nBu_4N]NO_3$ (0.005 g, 0.017 mmol, 1 equiv) was added to the solution as a solid. The reaction mixture was stirred for 24 h at 50 °C, after which the volatiles were removed under vacuum. Analytical data on the crude reaction mixture by electronic absorption spectra and CV revealed that the product was a mixture of $2\text{-}V_6O_7^{2-}$ and $5\text{-}V_6O_7^{1-}$.[38,39]

Synthesis of $[V_6O_6(OC_2H_5)_{12}(NO_3)]^{1-}$ ($8\text{-}V_6O_6NO_3^{1-}$). In a glovebox, a 20 mL scintillation vial was charged with $4\text{-}V_6O_6^0$ (0.035 g, 0.036 mmol) and 6 mL of dichloromethane. $[^nBu_4N]NO_3$ (0.012 g, 0.039 mmol, 1.1 equiv) was added to the solution as a solid. The reaction mixture was stirred for 1 h at 21 °C, after which the volatiles were removed under vacuum to yield $8\text{-}V_6O_6NO_3^{1-}$. ^{1}H NMR (400 MHz, $CDCl_3$): δ 28.73 (fwhh = 344 Hz), 22.37 (fwhh = 312 Hz), −0.45 (fwhh = 128 Hz), −2.42 (fwhh = 164 Hz), −23.69 (fwhh = 768 Hz). FT-IR (ATR, cm^{-1}): 1462 (NO_3), 1300 (NO_3), 1042 (O−C_2H_5), 957 (V═O).

Nitrate Reduction with $V_6O_6(OC_2H_5)_{12}(CH_3CN)$ ($4\text{-}V_6O_6^0$). In a glovebox, a 20 mL scintillation vial was charged with $4\text{-}V_6O_6^0$ (0.045 g, 0.046 mmol) and 8 mL of tetrahydrofuran. $[^nBu_4N]NO_3$ (0.014 g, 0.046 mmol, 1 equiv) was added to the solution as a solid. The reaction mixture was stirred for 1.5 h at 50 °C, after which the volatiles were removed under vacuum. Analytical data on the crude reaction mixture by electronic absorption spectra and CV revealed that the product was a mixture of $5\text{-}V_6O_7^{1-}$ and $7\text{-}V_6O_7^0$.[38,39]

Nitrate Reduction with $V_6O_6(OC_2H_5)_{12}$OTf ($6\text{-}V_6O_6^{1+}$). In a glovebox, a 20 mL scintillation vial was charged with $6\text{-}V_6O_6^{1+}$ (0.021 g, 0.019 mmol) and 8 mL of tetrahydrofuran. $[^nBu_4N]NO_3$ (0.006 g, 0.020 mmol, 1 equiv) was added to the solution as a solid. The reaction mixture was stirred for 4 days at 50 °C, after which the volatiles were removed under vacuum. Analytical data on the crude reaction mixture by electronic absorption spectra and CV revealed that the product was a mixture of $7\text{-}V_6O_7^0$ and $9\text{-}V_6O_7^{1+}$.[38,39]

■ ASSOCIATED CONTENT

Supporting Information

The Supporting Information is available free of charge at https://pubs.acs.org/doi/10.1021/acs.inorgchem.0c02052.

^{1}H NMR, IR, and electronic absorption spectra as well as cyclic voltammograms of all NO_x^- reduction reactions, CoTPP control experiments, ^{1}H NMR and absorption spectra of in situ NO-trapping experiments, ^{1}H NMR, IR, and ESI-MS of complexes $3\text{-}V_6O_6NO^{1-}$ and $8\text{-}V_6O_6NO_3^{1-}$ (PDF)

■ AUTHOR INFORMATION

Corresponding Author

Ellen M. Matson − *Department of Chemistry, University of Rochester, Rochester, New York 14627, United States;* orcid.org/0000-0003-3753-8288; Email: matson@chem.rochester.edu

Author

Brittney E. Petel − *Department of Chemistry, University of Rochester, Rochester, New York 14627, United States*

Complete contact information is available at: https://pubs.acs.org/10.1021/acs.inorgchem.0c02052

Author Contributions

The manuscript was written through contributions of all authors. All authors have given approval to the final version of the manuscript.

Funding

This research was funded by the National Science Foundation through Grant CHE-1653195. The authors also acknowledge financial support from the University of Rochester.

Notes

The authors declare no competing financial interest.

■ REFERENCES

(1) Holm, R. H. Metal-centered oxygen atom transfer reactions. *Chem. Rev.* **1987**, *87* (6), 1401−1449.

(2) Kay Lup, A. N.; Abnisa, F.; Wan Daud, W. M. A.; Aroua, M. K. A review on reactivity and stability of heterogeneous metal catalysts for deoxygenation of bio-oil model compounds. *J. Ind. Eng. Chem.* **2017**, *56*, 1−34.

(3) Ruiz Puigdollers, A.; Schlexer, P.; Tosoni, S.; Pacchioni, G. Increasing Oxide Reducibility: The Role of Metal/Oxide Interfaces in the Formation of Oxygen Vacancies. *ACS Catal.* **2017**, *7* (10), 6493−6513.

(4) Mars, P.; van Krevelen, D. W. Oxidations carried out by means of vanadium oxide catalysts. *Chem. Eng. Sci.* **1954**, *3*, 41−59.
(5) Doornkamp, C.; Ponec, V. The universal character of the Mars and Van Krevelen mechanism. *J. Mol. Catal. A: Chem.* **2000**, *162* (1), 19−32.
(6) Hermann, K.; Witko, M.; Druzinic, R.; Tokarz, R. Oxygen vacancies at oxide surfaces: ab initio density functional theory studies on vanadium pentoxide. *Appl. Phys. A: Mater. Sci. Process.* **2001**, *72* (4), 429−442.
(7) Ganduglia-Pirovano, M. V.; Hofmann, A.; Sauer, J. Oxygen vacancies in transition metal and rare earth oxides: Current state of understanding and remaining challenges. *Surf. Sci. Rep.* **2007**, *62* (6), 219−270.
(8) Zhang, J.; Zhao, Z.; Li, J.; Jin, H.; Rehman, F.; Chen, P.; Jiang, Y.; Chen, C.; Cao, M.; Zhao, Y. Evolution of Structural and Electrical Properties of Oxygen-Deficient VO2 under Low Temperature Heating Process. *ACS Appl. Mater. Interfaces* **2017**, *9* (32), 27135−27141.
(9) Jeong, J.; Aetukuri, N.; Graf, T.; Schladt, T. D.; Samant, M. G.; Parkin, S. S. P. Suppression of Metal-Insulator Transition in VO^2 by Electric Field−Induced Oxygen Vacancy Formation. *Science* **2013**, *339* (6126), 1402.
(10) Chen, L.; Cui, Y.; Shi, S.; Liu, B.; Luo, H.; Gao, Y. First-principles study of the effect of oxygen vacancy and strain on the phase transition temperature of VO2. *RSC Adv.* **2016**, *6* (90), 86872−86879.
(11) Heuer-Jungemann, A.; Feliu, N.; Bakaimi, I.; Hamaly, M.; Alkilany, A.; Chakraborty, I.; Masood, A.; Casula, M. F.; Kostopoulou, A.; Oh, E.; Susumu, K.; Stewart, M. H.; Medintz, I. L.; Stratakis, E.; Parak, W. J.; Kanaras, A. G. The Role of Ligands in the Chemical Synthesis and Applications of Inorganic Nanoparticles. *Chem. Rev.* **2019**, *119* (8), 4819−4880.
(12) Rambukwella, M.; Sakthivel, N. A.; Delcamp, J. H.; Sementa, L.; Fortunelli, A.; Dass, A. Ligand Structure Determines Nanoparticles' Atomic Structure, Metal-Ligand Interface and Properties. *Front. Chem.* **2018**, *6*, 330.
(13) Ling, D.; Hackett, M. J.; Hyeon, T. Surface ligands in synthesis, modification, assembly and biomedical applications of nanoparticles. *Nano Today* **2014**, *9* (4), 457−477.
(14) Rossi, L. M.; Fiorio, J. L.; Garcia, M. A. S.; Ferraz, C. P. The role and fate of capping ligands in colloidally prepared metal nanoparticle catalysts. *Dalton Transactions* **2018**, *47* (17), 5889−5915.
(15) Lian, S.; Kodaimati, M. S.; Weiss, E. A. Photocatalytically Active Superstructures of Quantum Dots and Iron Porphyrins for Reduction of CO2 to CO in Water. *ACS Nano* **2018**, *12* (1), 568−575.
(16) Edwards, E. H.; Fertig, A. A.; McClelland, K. P.; Meidenbauer, M. T.; Chakraborty, S.; Krauss, T. D.; Bren, K. L.; Matson, E. Enhancing the activity of photocatalytic hydrogen evolution from CdSe quantum dots with a polyoxovanadate cluster. *Chem. Commun.* **2020**, *56*, 8762.
(17) Zhang, T.; Sole-Daura, A.; Hostachy, S.; Blanchard, S.; Paris, C.; Li, Y.; Carbo, J. J.; Poblet, J. M.; Proust, A.; Guillemot, G. Modeling the Oxygen Vacancy at a Molecular Vanadium(III) Silica-Supported Catalyst. *J. Am. Chem. Soc.* **2018**, *140* (44), 14903−14914.
(18) Efremenko, I.; Neumann, R. Computational Insight into the Initial Steps of the Mars−van Krevelen Mechanism: Electron Transfer and Surface Defects in the Reduction of Polyoxometalates. *J. Am. Chem. Soc.* **2012**, *134* (51), 20669−20680.
(19) Khenkin, A. M.; Leitus, G.; Neumann, R. Electron Transfer-Oxygen Transfer Oxygenation of Sulfides Catalyzed by the H5PV2Mo10O40 Polyoxometalate. *J. Am. Chem. Soc.* **2010**, *132* (33), 11446−11448.
(20) Khenkin, A. M.; Neumann, R. Low-Temperature Activation of Dioxygen and Hydrocarbon Oxidation Catalyzed by a Phosphovanadomolybdate: Evidence for a Mars−van Krevelen Type Mechanism in a Homogeneous Liquid Phase. *Angew. Chem., Int. Ed.* **2000**, *39* (22), 4088−4090.
(21) Neumann, R.; Khenkin, A. M. Molecular oxygen and oxidation catalysis by phosphovanadomolybdates. *Chem. Commun.* **2006**, No. 24, 2529−2538.
(22) Khenkin, A. M.; Weiner, L.; Wang, Y.; Neumann, R. Electron and Oxygen Transfer in Polyoxometalate, H5PV2Mo10O40, Catalyzed Oxidation of Aromatic and Alkyl Aromatic Compounds: Evidence for Aerobic Mars-van Krevelen-Type Reactions in the Liquid Homogeneous Phase. *J. Am. Chem. Soc.* **2001**, *123* (35), 8531−8542.
(23) Khenkin, A. M.; Neumann, R. Oxidative C-C Bond Cleavage of Primary Alcohols and Vicinal Diols Catalyzed by H5PV2Mo10O40 by an Electron Transfer and Oxygen Transfer Reaction Mechanism. *J. Am. Chem. Soc.* **2008**, *130* (44), 14474−14476.
(24) Goldberg, H.; Kaminker, I.; Goldfarb, D.; Neumann, R. Oxidation of Carbon Monoxide Cocatalyzed by Palladium(0) and the H5PV2Mo10O40 Polyoxometalate Probed by Electron Paramagnetic Resonance and Aerobic Catalysis. *Inorg. Chem.* **2009**, *48* (16), 7947−7952.
(25) Sarma, B. B.; Carmieli, R.; Collauto, A.; Efremenko, I.; Martin, J. M. L.; Neumann, R. Electron Transfer Oxidation of Benzene and Aerobic Oxidation to Phenol. *ACS Catal.* **2016**, *6* (10), 6403−6407.
(26) Tsui, E. Y.; Kanady, J. S.; Agapie, T. Synthetic Cluster Models of Biological and Heterogeneous Manganese Catalysts for O2 Evolution. *Inorg. Chem.* **2013**, *52* (24), 13833−13848.
(27) Sarma, B. B.; Efremenko, I.; Neumann, R. Oxygenation of Methylarenes to Benzaldehyde Derivatives by a Polyoxometalate Mediated Electron Transfer−Oxygen Transfer Reaction in Aqueous Sulfuric Acid. *J. Am. Chem. Soc.* **2015**, *137* (18), 5916−5922.
(28) Hayashi, Y. Hetero and lacunary polyoxovanadate chemistry: Synthesis, reactivity and structural aspects. *Coord. Chem. Rev.* **2011**, *255* (19−20), 2270−2280.
(29) Wang, S. S.; Yang, G. Y. Recent advances in polyoxometalate-catalyzed reactions. *Chem. Rev.* **2015**, *115* (11), 4893−962.
(30) Petel, B. E.; Matson, E. M. Conversion of NOx1- (x = 2, 3) to NO using an oxygen-deficient polyoxovanadate−alkoxide cluster. *Chem. Commun.* **2020**, *56* (4), 555−558.
(31) Petel, B. E.; Brennessel, W. W.; Matson, E. M. Oxygen-Atom Vacancy Formation at Polyoxovanadate Clusters: Homogeneous Models for Reducible Metal Oxides. *J. Am. Chem. Soc.* **2018**, *140* (27), 8424−8428.
(32) Petel, B. E.; Meyer, R. L.; Brennessel, W. W.; Matson, E. M. Oxygen atom transfer with organofunctionalized polyoxovanadium clusters: O-atom vacancy formation with tertiary phosphanes and deoxygenation of styrene oxide. *Chemical Science* **2019**, *10* (34), 8035−8045.
(33) Petel, B. E.; Fertig, A. A.; Maiola, M. L.; Brennessel, W. W.; Matson, E. M. Controlling Metal-to-Oxygen Ratios via M═O Bond Cleavage in Polyoxovanadate Alkoxide Clusters. *Inorg. Chem.* **2019**, *58*, 10462.
(34) Schreiber, E.; Petel, B. E.; Matson, E. M. Acid-Induced, Oxygen-Atom Defect Formation in Reduced Polyoxovanadate-Alkoxide Clusters. *J. Am. Chem. Soc.* **2020**, *142* (22), 9915−9919.
(35) Maiola, M. L.; Petel, B. E.; Brennessel, W. W.; Matson, E. M., Site-selective halogenation of mixed-valent vanadium oxide clusters. *Dalton Trans.* **2020**. DOI: 10.1039/D0DT01077D
(36) Petel, B. E.; Meyer, R. L.; Maiola, M. L.; Brennessel, W. W.; Müller, A. M.; Matson, E. M. Site-Selective Halogenation of Polyoxovanadate Clusters: Atomically Precise Models for Electronic Effects of Anion Doping in VO2. *J. Am. Chem. Soc.* **2020**, *142* (2), 1049−1056.
(37) VanGelder, L. E.; Kosswattaarachchi, A. M.; Forrestel, P. L.; Cook, T. R.; Matson, E. M. Polyoxovanadate-alkoxide clusters as multi-electron charge carriers for symmetric non-aqueous redox flow batteries. *Chemical Science* **2018**, *9* (6), 1692−1699.
(38) Daniel, C.; Hartl, H. Neutral and Cationic VIV/VV Mixed-Valence Alkoxo-polyoxovanadium Clusters [V6O7(OR)12]n+ (R = -CH3, -C2H5): Structural, Cyclovoltammetric and IR-Spectroscopic Investigations on Mixed Valency in a Hexanuclear Core. *J. Am. Chem. Soc.* **2005**, *127* (40), 13978−13987.

https://dx.doi.org/10.1021/acs.inorgchem.0c02052
Inorg. Chem. 2021, 60, 6855−6864

(39) Daniel, C.; Hartl, H. A Mixed-Valence VIV/VV Alkoxo-polyoxovanadium Cluster Series [V6O8(OCH3)11]n±: Exploring the Influence of a μ-Oxo Ligand in a Spin Frustrated Structure. *J. Am. Chem. Soc.* **2009**, *131* (14), 5101−5114.
(40) Li, F.; Meyer, R. L.; Carpenter, S. H.; VanGelder, L. E.; Nichols, A. W.; Machan, C. W.; Neidig, M. L.; Matson, E. M. Nitric oxide activation facilitated by cooperative multimetallic electron transfer within an iron-functionalized polyoxovanadate−alkoxide cluster. *Chemical Science* **2018**, *9* (30), 6379−6389.
(41) Mallik, M.; Ghosh, P. N.; Bhattacharyya, R. Generation of the V(NO)2+ moiety from VO43− using hydroxylamine and pseudo-halide ions: synthesis and electrochemistry of [V(NO)2(L−L)2]X (L−L = 2,2′-bipyridine or 1,10-phenanthroline). *J. Chem. Soc., Dalton Trans.* **1993**, No. 11, 1731−1736.
(42) Hayton, T. W.; Patrick, B. O.; Legzdins, P. Reactivity of (trimpsi)V(NO)X2 Complexes (X = Cl, Br, I; trimpsi = tBuSi-(CH2PMe2)3). Synthesis of the First Group 5 Alkyl Nitrosyls. *Organometallics* **2004**, *23* (4), 657−664.
(43) Cioncoloni, G.; Roger, I.; Wheatley, P. S.; Wilson, C.; Morris, R. E.; Sproules, S.; Symes, M. D. Proton-Coupled Electron Transfer Enhances the Electrocatalytic Reduction of Nitrite to NO in a Bioinspired Copper Complex. *ACS Catal.* **2018**, *8* (6), 5070−5084.
(44) Moore, C. M.; Szymczak, N. K. Nitrite reduction by copper through ligand-mediated proton and electron transfer. *Chemical Science* **2015**, *6* (6), 3373−3377.
(45) Kumar, M.; Dixon, N. A.; Merkle, A. C.; Zeller, M.; Lehnert, N.; Papish, E. T. Hydrotris(triazolyl)borate Complexes as Functional Models for Cu Nitrite Reductase: The Electronic Influence of Distal Nitrogens. *Inorg. Chem.* **2012**, *51* (13), 7004−7006.
(46) Bartberger, M. D.; Liu, W.; Ford, E.; Miranda, K. M.; Switzer, C.; Fukuto, J. M.; Farmer, P. J.; Wink, D. A.; Houk, K. N. The reduction potential of nitric oxide (NO) and its importance to NO biochemistry. *Proc. Natl. Acad. Sci. U. S. A.* **2002**, *99* (17), 10958.
(47) Yoo, C.; Dodge, H. M.; Miller, A. J. M. Cation-controlled catalysis with crown ether-containing transition metal complexes. *Chem. Commun.* **2019**, *55* (35), 5047−5059.
(48) Cai, Z.; Xiao, D.; Do, L. H. Fine-Tuning Nickel Phenoxyimine Olefin Polymerization Catalysts: Performance Boosting by Alkali Cations. *J. Am. Chem. Soc.* **2015**, *137* (49), 15501−15510.
(49) Chantarojsiri, T.; Reath, A. H.; Yang, J. Y. Cationic Charges Leading to an Inverse Free-Energy Relationship for N-N Bond Formation by MnVI Nitrides. *Angew. Chem., Int. Ed.* **2018**, *57* (43), 14037−14042.
(50) Burns, K. T.; Marks, W. R.; Cheung, P. M.; Seda, T.; Zakharov, L. N.; Gilbertson, J. D. Uncoupled Redox-Inactive Lewis Acids in the Secondary Coordination Sphere Entice Ligand-Based Nitrite Reduction. *Inorg. Chem.* **2018**, *57* (16), 9601−9610.
(51) de Ruiter, G.; Carsch, K. M.; Gul, S.; Chatterjee, R.; Thompson, N. B.; Takase, M. K.; Yano, J.; Agapie, T. Accelerated Oxygen Atom Transfer and C-H Bond Oxygenation by Remote Redox Changes in Fe3Mn-Iodosobenzene Adducts. *Angew. Chem., Int. Ed.* **2017**, *56* (17), 4772−4776.
(52) Reed, C. J.; Agapie, T. A Terminal FeIII−Oxo in a Tetranuclear Cluster: Effects of Distal Metal Centers on Structure and Reactivity. *J. Am. Chem. Soc.* **2019**, *141* (24), 9479−9484.
(53) Arnett, C. H.; Chalkley, M. J.; Agapie, T. A Thermodynamic Model for Redox-Dependent Binding of Carbon Monoxide at Site-Differentiated, High Spin Iron Clusters. *J. Am. Chem. Soc.* **2018**, *140* (16), 5569−5578.
(54) Reed, C. J.; Agapie, T. Thermodynamics of Proton and Electron Transfer in Tetranuclear Clusters with Mn−OH2/OH Motifs Relevant to H2O Activation by the Oxygen Evolving Complex in Photosystem II. *J. Am. Chem. Soc.* **2018**, *140* (34), 10900−10908.
(55) de Ruiter, G.; Thompson, N. B.; Lionetti, D.; Agapie, T. Nitric Oxide Activation by Distal Redox Modulation in Tetranuclear Iron Nitrosyl Complexes. *J. Am. Chem. Soc.* **2015**, *137* (44), 14094−14106.
(56) Xue, G.; De Hont, R.; Münck, E.; Que, L., Jr. Million-fold activation of the [Fe(2)(micro-O)(2)] diamond core for C-H bond cleavage. *Nat. Chem.* **2010**, *2* (5), 400−405.
(57) Holm, R. H.; Donahue, J. P. A thermodynamic scale for oxygen atom transfer reactions. *Polyhedron* **1993**, *12* (6), 571−589.
(58) Wagman, D. D. *He Nbs Tables of Chemical Thermodynamic Properties: Selected Values for Inorganic and C_1 and C_2 Organic Substances in Si Units*; American Chemical Society and the American Institute of Physics for the National Bureau of Standards: Washington, DC, 1982.
(59) Addison, C. C.; Gatehouse, B. M. The infrared spectra of anhydrous transition-metal nitrates. *J. Chem. Soc.* **1960**, *125* (0), 613−616.
(60) Patil, K. C.; Nesamani, C.; Pai Verneker, V. R. Synthesis and Characterisation of Metal Hydrazine Nitrate, Azide and Perchlorate Complexes. *Synth. React. Inorg. Met.-Org. Chem.* **1982**, *12* (4), 383−395.
(61) Ford, C. L.; Park, Y. J.; Matson, E. M.; Gordon, Z.; Fout, A. R. A bioinspired iron catalyst for nitrate and perchlorate reduction. *Science* **2016**, *354* (6313), 741.

https://dx.doi.org/10.1021/acs.inorgchem.0c02052
Inorg. Chem. 2021, 60, 6855−6864